PEXSI-Σ: A GREEN'S FUNCTION EMBEDDING METHOD FOR KOHN-SHAM DENSITY FUNCTIONAL THEORY

XIANTAO LI, LIN LIN, AND JIANFENG LU

Abstract. As Kohn-Sham density functional theory (KSDFT) being applied to increasingly more complex materials, the periodic boundary condition associated with supercell approaches also becomes unsuitable for a number of important scenarios. Green's function embedding methods allow a more versatile treatment of complex boundary conditions, and hence provide an attractive alternative to describe complex systems that cannot be easily treated in supercell approaches. In this paper, we first revisit the literature of Green's function embedding methods from a numerical linear algebra perspective. We then propose a new Green's function embedding method called PEXSI-Σ. The PEXSI-Σ method approximates the density matrix using a set of nearly optimally chosen Green's functions evaluated at complex frequencies. For each Green's function, the complex boundary conditions are described by a self energy matrix Σ constructed from a physical reference Green's function, which can be computed relatively easily. In the linear regime, such treatment of the boundary condition can be numerically exact. The support of the Σ matrix is restricted to degrees of freedom near the surface of computational domain, and can be interpreted as a frequency dependent surface potential. This makes it possible to perform KSDFT calculations with $\mathcal{O}(N^2)$ computational complexity, where N is the number of atoms within the computational domain. Green's function embedding methods are also naturally compatible with atomic-level Green's function methods for relaxing the atomic configuration outside the computational domain. As a proof of concept, we demonstrate the accuracy of the PEXSI-Σ method for graphene with divacancy and dislocation dipole type of defects using the DFTB+ software package.

1. Introduction

In the past two decades, supercell approaches such as those based on planewave basis sets [30, 46] have been the most widely used methods in computational materials science in the framework of Kohn-Sham density functional theory (KSDFT) [17, 29]. Supercell approaches can treat both large basis sets such as planewaves, and reasonably large system sizes up to hundreds to thousands of atoms. Supercell approaches are also convenient to use in the sense that a unified procedure can be applied to systems with or without defects [42]. On the other hand, the inherent periodic boundary treatment in supercell approaches is not always suitable. Quantum transport, defect migration, defect-defect interaction, and dislocation are just a few examples of scenarios where the periodic boundary condition encounters difficulties.

The work of X.L. was supported by the National Science Foundation under award DMS-1522617. The work of L.L. was partially supported by Laboratory Directed Research and Development (LDRD) funding from Berkeley Lab, provided by the Director, Office of Science, of the U.S. Department of Energy under Contract No. DE-AC02-05CH11231, the Alfred P. Sloan foundation, the DOE Scientific Discovery through the Advanced Computing (SciDAC) program and the DOE Center for Applied Mathematics for Energy Research Applications (CAMERA) program. The work of J.L. was supported in part by the National Science Foundation under awards DMS-1312659 and DMS-1454939.

In order to model perturbations in materials (henceforth generally referred to as "defects") without enforcing periodic boundary conditions, it is desirable to "embed" the defects into the underlying environment, and to incorporate environmental effects by means of appropriate and more versatile boundary conditions. Various embedding schemes [9, 12, 16, 21, 27] have been developed in the literature in order to model complex materials more efficiently. Such methods allow the defect region to be treated not only at the level of KSDFT, but also at higher levels of quantum theories such as the coupled cluster theory, though the accuracy of the latter approach of embedding is significantly more difficult to analyze from a numerical analysis perspective. In this paper we focus on Green's function methods [3, 8, 26, 54, 55, 58], and treat the defect region at the level of KSDFT. Green's function methods allow a more versatile treatment of complex boundary conditions, and hence provide an attractive alternative to describe complex systems. However, a notable disadvantage of conventional Green's function methods for planewave basis sets is that they require the inversion of many dense matrices, which arises from discretization points of a contour in the complex plane. Thus for large systems, localized basis sets are necessary. To overcome the computational cost of inverting large matrices, Green's function methods have been combined with localization based methods to achieve linear scaling complexity for solving KSDFT for insulating systems. Examples include the locally self-consistent multiple scattering (LSMS) method [45,52], Fermi operator expansion method [14,15], and the recent extension of the Korringa-Kohn-Rostoker (KKR) method [56,57] called KKRnano [49].

The recently developed pole expansion and selected inversion method (PEXSI) [34, 36], which is also a Green's function method, is a promising candidate for accelerating KSDFT calculations especially for metallic systems. The PEXSI method has two key components. First, PEXSI uses the pole expansion [37] for approximating the one-particle density matrix by means of an efficient rational approximation, and hence the density matrix is approximated by the linear combination of a relatively small number of Green's functions. For a system with inverse temperature β and spectral radius ΔE, the number of Green's functions needed by the pole expansion is asymptotically only $\mathcal{O}(\log \beta \Delta E)$ (usually 40-80 is sufficient). Second, PEXSI uses the selected inversion method [36,39] to directly compute the entries of each Green's function corresponding to the sparsity pattern of Kohn-Sham Hamiltonian H, and avoids the computation of any eigenvalue or eigenfunction of H. The selected inversion method does not rely on the near-sightedness principle [28], but only relies on the sparsity of the H, S matrices. Hence the PEXSI method is applicable to metallic systems at room temperature. The computational complexity of the selected inversion method is at most $\mathcal{O}(N^2)$ for 3D bulk systems, and is sub-quadratic for lower dimensional systems. Further, the PEXSI method can be scalable on massively parallel computers [23,24]. PEXSI has been integrated into a number of electronic structure software packages such as SIESTA [35,48], BigDFT [44], CP2K [51] and DGDFT [18,38], and has been used for accelerating materials simulation with 10000 atoms or more [19,20].

The main contribution of our work is to propose a new Green's function embedding method called PEXSI-Σ, which is a natural extension of PEXSI to impose the boundary condition for the Green's functions in the defect region. We consider local defects embedded in a physical reference system such as a crystal. Our assumption is that we can obtain the Green's function G^0 for the reference system (*e.g.*, by means of a band structure calculation using the periodicity of the reference problem). The key idea of our approach is to obtain the boundary condition of the perturbed system via a Schur complement, which can be readily calculated by the reference Green's function G^0. If the problem is linear (*e.g.*, for a model Hamiltonian without self-consistent field iteration), our scheme in fact provides the

numerically exact density matrix restricted to the defect region, and there is no error if the physical observable, such as the atomic force, only depends the local electronic structure. The modified boundary condition is a Σ matrix that is only nonzero at the degrees of freedom near the surface of the defect region, and hence it can be interpreted as a surface potential, which might be embedding

We would like to point out that the Σ matrix is closely related to the self energy matrix in the non-equilibrium Green's function (NEGF) method in quantum transport calculations [5]. The important difference is that NEGF calculations typically require the solution of quasi one-dimensional semi-infinite problems corresponding to the metallic leads, which can be solved efficiently by the recursive Green's function method [40], which can be viewed as a special case of the selected inversion method for quasi one-dimensional systems. In the context of modeling local defects, this strategy would require the solution of a system with a "hole" corresponding to the defect region, which can be as difficult to solve as the original problem. In fact, we think our strategy for constructing Σ matrices could be potentially beneficial in the context of quantum transport calculations as well. Our method is also related to the embedding method proposed by Inglesfield [22], which is based on matching the boundary condition for each individual eigenfunction. This strategy could be viable when eigenfunctions are well separated from each other. However, when eigenfunctions are clustered such as for large scale KSDFT calculations, it becomes impractical to derive the boundary condition for each eigenfunction. Mathematically, our approach is closely related to the Dirichlet-to-Neumann (DtN) map, which has been successfully obtained or approximated in various contexts [10, 13, 25]. To the extent of our knowledge, the construction of such DtN type operator has not been presented in the electronic structure literature. Furthermore, we extend the Green's function embedding method to structural relaxation using the recently developed atomic Dirichlet-to-Neumann scheme [32].

We note that the spirit of Green's function embedding methods are very different from that of the quantum mechanics / molecular mechanics (QM/MM) method, which is widely used in chemistry and biology [53]. In the QM/MM method, the coupling of the two types of models is usually a significant challenge. While QM models involve the degrees of freedom associated with electrons (for example, electron density or electron orbital functions), MM models do not explicitly take into account those degrees of freedom. One intuitive way to understand the issue at the boundary is that the decomposition of the domain into QM and MM regions creates "dangling bonds" at the interface. Therefore, a popular approach is to introduce hydrogen-type atoms to passivate those bonds. More advanced approaches have been proposed to further reduce the artifacts introduced by the coupling. See for example the review articles [6, 11, 33, 47]. We remark that the bond passivation model becomes challenging in materials science simulations, such as the description of a local defect in aluminum. In Green's function embedding methods, the coupling is through the boundary conditions imposed on the Green's function of the QM domain, rather than changing the local chemical environment of the coupling region. In particular, no bond passivation is required.

As a proof of concept, we implement the PEXSI-Σ method in the DFTB+ software package [1], and demonstrate the accuracy using a water dimer, graphene with divacancy, and graphene with a dislocation dipole with relaxed geometric structure in the context of non self-consistent field iteration. Our numerical results indicate that the use of the Σ matrices leads to significantly improved description of the energy and forces.

The manuscript is organized as follows. We briefly introduce Kohn-Sham density functional theory and Green's function methods in section 2. In section 3 we review existing

Green's function methods from a numerical linear algebra perspective, and introduce the PEXSI-Σ method. We report the numerical results using DFTB+ in section 5, and discuss future directions in section 6.

2. Preliminaries

In Kohn-Sham density functional theory, the ground-state electron charge density $\rho(x)$ of an atomistic system can be obtained from the self-consistent solution to the Kohn-Sham equations

$$\widehat{H}\left[\rho\right]\psi_i(x) = \psi_i(x)\varepsilon_i, \tag{1}$$

where $\widehat{H}$ is the Kohn-Sham Hamiltonian that depends on ρ, and $\{\psi_i(x)\}$ are the Kohn-Sham orbitals. The Kohn-Sham orbitals in turn determine the charge density by

$$\rho(x) = \sum_{i=1}^{\infty} |\psi_i(x)|^2 f_i. \tag{2}$$

The occupation numbers $\{f_i\}$ are chosen according to the Fermi-Dirac distribution function

$$f_i = f_\beta(\varepsilon_i - \mu) = \frac{2}{1 + e^{\beta(\varepsilon_i - \mu)}}, \tag{3}$$

where μ is the chemical potential chosen to ensure that

$$\int \rho(x)\,\mathrm{d}x = N_e. \tag{4}$$

β is the inverse temperature, i.e., $\beta = 1/(k_B T)$ with k_B being the Boltzmann constant and T the temperature.

The electronic-structure problem can be recast in terms of the one-particle density matrix defined by

$$\widehat{\Gamma} = \sum_{i=1}^{\infty} |\psi_i\rangle f_\beta(\varepsilon_i - \mu)\langle\psi_i| = f_\beta(\widehat{H} - \mu), \tag{5}$$

and the chemical potential μ chosen so that $\mathrm{Tr}\,\widehat{\Gamma} = N_e$, which is exactly the same constraint as (4).

To solve for ρ or $\widehat{\Gamma}$ in practice, we may choose a finite basis set $\{\varphi_j\}$, and use a Galerkin approximation for (1) as the generalized eigenvalue problem

$$H[\rho]C = SC\Xi, \tag{6}$$

where $H_{ij} = \langle\varphi_i|\widehat{H}|\varphi_j\rangle$ is the projected Hamiltonian matrix, and $S_{ij} = \langle\varphi_i|\varphi_j\rangle$ is the overlap matrix. The matrix representation of the density matrix, denoted by Γ, can be obtained from the generalized eigenvalue decomposition (6) as

$$\Gamma = C f_\beta(\Xi - \mu)C^T. \tag{7}$$

For simplicity we consider the case when real arithmetic is used, and H, S, Γ are real symmetric matrices. The extension to the complex Hermitian case is straightforward. Using linear algebra notation, let us denote by $\Phi = [\varphi_1, \cdots, \varphi_N]$ the matrix collecting all N basis functions. Then the density matrix in the real space can be compactly approximated by

$$\widehat{\Gamma} \approx \Phi\Gamma\Phi^T. \tag{8}$$

It turns out that, in KSDFT calculations with the local density approximation (LDA) and generalized gradient approximation (GGA) for the exchange-correlation functionals, not all

entries of the one-particle density matrix are needed. In order to carry out the self-consistent field iteration, it is sufficient to compute the electron density ρ, the diagonal entries of $\widehat{\Gamma}$ in the real space, i.e.,

$$\rho(x) \approx \Phi(x)\Gamma\Phi^T(x) = \sum_{ij} \Gamma_{ij}\varphi_j(x)\varphi_i(x). \tag{9}$$

When the basis functions $\varphi_i(x)$ are compactly supported in real space, the product of two functions $\varphi_i(x)$ and $\varphi_j(x)$ will be zero when they do not overlap. This leads to sparse Hamiltonian matrix H and overlap matrix S, respectively. It also implies that in order to compute $\rho(x)$, we only need Γ_{ij} such that $\varphi_j(x)\varphi_i(x) \neq 0$ in Eq. (9). As shall be seen later, such sparsity plays a key role in our method.

The Kohn-Sham equations (1) are well-defined for closed systems such as systems in vacuum (i.e., with Dirichlet boundary condition imposed far away from the system) and with periodic boundary condition. However, the eigenvalue formulation imposes major difficulty for treating *open* systems. For instance, the embedding of a defect into a crystalline system, which can be a point defect such as a vacancy, or a line defect such as a dislocation. As opposed to the solution of PDEs where tailored boundary conditions can be formulated for specific operators such as in the case of the absorbing boundary condition [10], in KSDFT each eigenfunction satisfies a different PDE, and hence requires its own tailored boundary condition. The number of eigenfunctions is proportional to the number of electrons N_e. Finding such boundary conditions is not only expensive when N_e becomes large, but also may not be stable since the eigenvalues of interest are often clustered, or even form continuous energy bands in the thermodynamic limit for solid state systems.

Here we demonstrate that the one-particle density matrix can serve as a useful tool for quantum embedding. First, $\widehat{\Gamma}$ can be evaluated without the need for diagonalization, if the Fermi function is approximated by a linear combination of a number of simpler functions. This is the idea behind the Fermi operator expansion (FOE) method [14]. The FOE method is typically used as a linear scaling method to accelerate KSDFT calculations for insulating systems with substantial band gaps, or for general systems under very high temperature. The recently developed pole expansion and selected inversion (PEXSI) method extends the FOE method by means of an efficient rational approximation, and significantly accelerates KSDFT calculations for large scale metallic systems at room temperature [34, 36, 37, 39]. The PEXSI method does not rely on the near-sightedness principle [28], but only relies on the sparsity of the H, S matrices.

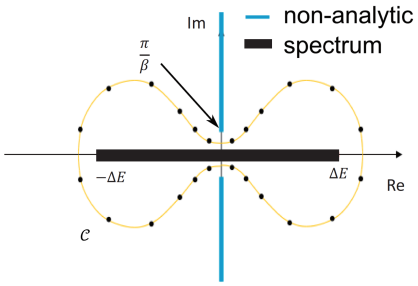

FIGURE 1. Sketch of the contour used in the PEXSI method.

In the PEXSI method, the single particle density matrix can be exactly reformulated by means of a contour integral as

$$\widehat{\Gamma}(x,x') = \frac{1}{2\pi i}\oint_{\mathcal{C}} f_\beta(z-\mu)(z-\widehat{H})^{-1}(x,x')\,\mathrm{d}z. \tag{10}$$

Here $\mathcal{C}$ can be any contour that encircles the spectrum of $\widehat{H}$ without enclosing any pole of the Fermi-Dirac function. In the pole expansion [37], we carefully choose a contour as in Fig. 1, and approximate the single particle density matrix $\widehat{\Gamma}$ by its P-term approximation, denoted by $\widehat{\Gamma}_P$ as

$$\begin{aligned}\widehat{\Gamma}_P(x,x') &= \Phi(x)\mathrm{Im}\left(\sum_{l=1}^{P}\frac{\omega_l^\rho}{(z_l+\mu)S-H}\right)\Phi^T(x') \\ &\equiv \Phi(x)\Gamma_P\Phi^T(x').\end{aligned} \tag{11}$$

The complex shifts $\{z_l\}$ and weights $\{\omega_l^\rho\}$ are determined only by $\beta, \Delta E$ (the spectrum width of the matrix pencil (H,S)) and the number of poles P. These coefficients are known explicitly and their calculation takes negligible amount of time. The pole expansion is an effective way for approximating the one-particle density matrix, since it requires only $\mathcal{O}(\log\beta\Delta E)$ terms of simple rational functions. With some abuse of notation, in the following discussion we will drop the subscript P originating from the P-term pole expansion approximation unless otherwise noted.

Eq. (11) converts the problem of computing the one-particle density matrix by means of eigenfunctions into a problem of evaluating P inverse matrices or *Green's functions*, defined as

$$G_l = \big((z_l+\mu)S-H\big)^{-1}, \quad l=1,\ldots,P. \tag{12}$$

In order to evaluate the electron density, we only need to evaluate the entries $(G_l)_{ij}$ such that $H_{ij}, S_{ij} \neq 0$. The selected inversion method [24,36,39] provides an efficient way of computing such *selected elements* of an inverse matrix. For a symmetric matrix of the form $A = zS-H$, the selected inversion algorithm first constructs an LDL^T factorization of A, where L is a block lower diagonal matrix called the Cholesky factor, and D is a block diagonal matrix. In the second step, the selected inversion algorithm computes all the elements A_{ij}^{-1} such that $L_{ij} \neq 0$. Since $L_{ij} \neq 0$ implies that $H_{ij}, S_{ij} \neq 0$, all the required selected elements of A^{-1} are computed, and the computational scaling of the selected inversion algorithm is only proportional to the number of nonzero elements in the Cholesky factor L. In particular, the selected inversion algorithm has the complexity of $\mathcal{O}(N)$ for quasi-1D systems, $\mathcal{O}(N^{1.5})$ for quasi-2D systems, and $\mathcal{O}(N^2)$ for 3D bulk systems. It should be noted that selected inversion algorithm is an *exact* method for computing selected elements of A^{-1} if exact arithmetic is to be employed, and in practice the only source of error is the roundoff error. In particular, the selected inversion algorithm does not rely on any localization property of A^{-1} [28]. However, it can be combined with localization properties of insulating systems to further reduce the computational cost. As a result, PEXSI can perform KSDFT calculations with at most $\mathcal{O}(N^2)$ asymptotic computational complexity. We also remark that the asymptotic complexity of selected inversion comes from the size of the largest dense matrix block in L. For a finite sized system, the size of this matrix block is approximately the same as the number of degrees of freedom corresponding to the surface of the system [36]. As will be seen later, this is an important property for the reduced computational complexity in the PEXSI-Σ method.

3. Green's function embedding schemes

In the context of embedding, we only need to find the boundary conditions for P Green's functions $\{G_l\}$, which correspond to P specific PDEs. Since P is independent of the system size N_e, this becomes a solvable problem even for systems of large sizes. On the other hand, finding proper boundary conditions for $\mathcal{O}(N_e)$ eigenvalue problems can become impractical for systems of large sizes [22]. In this section we first review some existing ideas in the literature, written in consistent linear algebra notation as used in the previous section. We then propose a new embedding scheme, referred to as the PEXSI-Σ method, in the same context as the previous methods.

In the embedding scheme, we partition the degrees of freedom (i.e., nodal values associated with the basis functions) into interior degrees of freedom Ω^i and exterior degrees of freedom Ω^e, where $\Omega^i \cap \Omega^e = \emptyset$. Parts of Ω^e are labeled as boundary degrees of freedom, denoted by $\partial\Omega^e$, such that $H(\Omega^i, \Omega^e \backslash \partial\Omega^e) = 0$ (locality of the Hamiltonian matrix is thus necessary). We also partition H into the block form

$$H = \begin{pmatrix} H_{11} & H_{12} \\ H_{21} & H_{22} \end{pmatrix}, \tag{13}$$

where $1, 2$ denotes $\Omega^i \cup \partial\Omega^e$ and $\Omega^e \backslash \partial\Omega^e$, respectively. Other matrices of the same size, such as the overlap matrix S and the density matrix Γ, can be partitioned accordingly. As will be seen below, grouping Ω^i and $\partial\Omega^e$ together allows accurate calculation of local physical quantities such as atomic forces corresponding to the degrees of freedom in Ω^i.

In this paper we assume atom-centered basis functions are used in discretizing the Hamiltonian operator. This is applicable to a number of practically used basis sets such as atomic orbitals, Gaussian type orbitals, as well as the density functional tight binding (DFTB) approximation [1], which will be used in our numerical examples. With some abuse of notation, we aggregate degrees of freedom corresponding to the single atom, as illustrated in Fig. 2, and perform the partition geometrically according to atomic positions. The atoms in Ω^i can be fully disordered and/or have defects, but we assume that the atomic configuration in Ω^e is not far away from relatively simple configurations, such as crystalline systems for which the Green's function can be evaluated or approximated without expensive computations. The quantity of interest is the density matrix restricted to Ω^i. To this end we need to evaluate Γ_{11}. We also require an embedding scheme to result in discretized systems involving only degrees of freedom in Ω^i, and the information from Ω^e will be incorporated implicitly.

Below we omit the subscript l (the index of the poles), and denote by

$$A = (z + \mu)S - H, \quad \text{and} \quad G = A^{-1}.$$

Note that the z dependence is implicit in the notation. The submatrices of G satisfy the equation

$$\begin{pmatrix} A_{11} & A_{12} \\ A_{21} & A_{22} \end{pmatrix} \begin{pmatrix} G_{11} & G_{12} \\ G_{21} & G_{22} \end{pmatrix} = \begin{pmatrix} I_1 & 0 \\ 0 & I_2 \end{pmatrix}, \tag{14}$$

where I_1, I_2 are identity matrices.

Green's function embedding methods typically involve two atomic configurations. We denote by H^0 and S^0 the matrices corresponding to a reference system, and H and S the matrices corresponding to a physical system of interest. For simplicity we assume that after discretization, the dimension of H^0 and H are the same. This assumption is clearly violated when atoms are added or removed from the systems. However, this condition can be relaxed in the practical numerical schemes as illustrated in section 3.3. We also assume that the

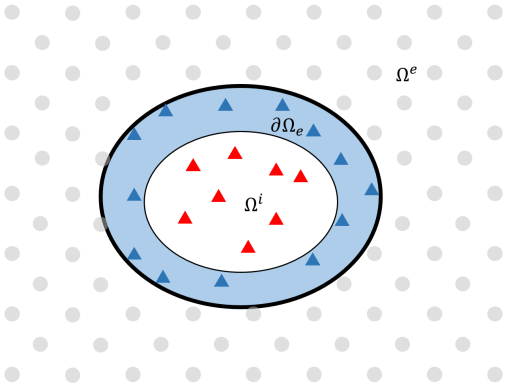

FIGURE 2. Partition of the atoms in the computation domain into interior domain Ω^i (red triangles), boundary between interior and exterior domain $\partial\Omega^e$ (blue triangles in shaded area), and the rest of the exterior domain $\Omega^e \backslash \partial\Omega^e$ (gray circles).

reference system and the physical system can be evaluated using the same contour, and define

$$A^0 = (z+\mu)S^0 - H^0.$$

In physical terms, this means that we choose the same chemical potential for the two systems. In this paper we assume the reference atomic configuration is a perfect crystal. In the presence of localized defect, it is possible to use such grand canonical ensemble treatment with fixed chemical potential. However, for finite sized reference systems, the grand canonical treatment is only an approximation, and update of the chemical potential to adjust for the correct number of electrons may become necessary.

3.1. **Schur complement method.** The most straightforward way to reduce the degrees of freedom in Ω^e is via the use of a Schur complement (a.k.a Gaussian elimination). The Schur complement method eliminates the A_{22} submatrix directly, and obtain

$$(A_{11} + \Sigma)\, G_{11} = I_1. \tag{15}$$

Here

$$\Sigma = -A_{12}A_{22}^{-1}A_{21}$$

is called the Schur complement, which reflects the impact of the exterior degrees of freedom to the interior degrees of freedom. The Schur complement Σ depends on the complex shift z. In physics literature, Σ is often referred to as the self energy matrix [5, 41]. The matrix inverse A_{22}^{-1} can be interpreted as the Green's function corresponding to a physical system with only degrees of freedom in $\Omega^e \backslash \partial\Omega^e$. In Fig. 2 this corresponds to the degrees of freedom represented by gray circles, which is a system containing a very large void by excluding the degrees of freedom in $\Omega^i \cup \partial\Omega^e$. In term of the reference system, the corresponding reference matrix A^0 takes the form

$$A^0 = \begin{pmatrix} 0 & 0 \\ 0 & A_{22} \end{pmatrix}.$$

For quasi-one-dimensional systems, the Schur complement method has been successfully applied in first principle quantum transport calculations using the non-equilibrium Green's

function methods [5]. In such calculations, the vacancy system becomes two independent semi-infinite systems, and can be calculated efficiently by means of recursive Green's function methods [40]. This technique becomes very costly for systems in two and three dimensions, since the cost of computing A_{22}^{-1} can be similar to that of the computation of the entire system.

3.2. **Dyson equation method.** To overcome the above mentioned difficulty associated with the Schur complement method, let us consider more general reference systems, with the requirement that they only differ with A in the A_{11} block, i.e.,

$$\Delta A := A^0 - A = \begin{pmatrix} A_{11}^0 - A_{11} & 0 \\ 0 & 0 \end{pmatrix}. \tag{16}$$

Nonetheless, even local changes in A_{11} can lead to extended changes in terms of the difference of Green's functions $G - G^0$. Green's function embedding methods can be regarded as approximations to solutions of G_{11} without the explicit involvement of the rest of blocks.

One possible way to achieve this is described by Williams, Feibelman and Lang [54], and later extended by Kelly and Car [26], through the Dyson's equation. Again using the same numerical linear algebra notation, here we demonstrate that the Dyson equation method can be interpreted equivalently using the Sherman-Morrison-Woodbury formula. Dyson's equation reads

$$G = G^0 + G^0 \Delta A G, \tag{17}$$

or equivalently

$$G = (I - G^0 \Delta A)^{-1} G^0.$$

We view ΔA as a "low-rank update" and rewrite as

$$\Delta A = e_1 (\Delta A)_{11} e_1^T,$$

where $e_1^T = [I_1, 0]$. Then by the Sherman-Morrison-Woodbury formula, we have,

$$G = G^0 + G^0 e_1 (\Delta A)_{11} (I_1 - (G^0)_{11} (\Delta A)_{11})^{-1} e_1^T G^0.$$

In order to evaluate the electron density in Ω^i, it is sufficient to evaluate G_{11} as

$$G_{11} = G_{11}^0 + G_{11}^0 (\Delta A)_{11} (I_1 - (G^0)_{11} (\Delta A)_{11})^{-1} G_{11}^0. \tag{18}$$

Note that all quantities, including the matrix inverse in Eq. (18) only involves matrices restricted to the degrees of freedom in Ω^i.

Compared to the Schur complement approach, one advantage of the Dyson equation approach is that the reference system can be chosen to be physically more meaningful for systems of all dimensions. In particular, for configurations such as the one in Fig. 2, Green's functions corresponding to the crystalline configuration can be efficiently computed by means of a band structure calculation, and can be readily used in Eq. (18).

Another advantage of the Dyson equation approach is that physical quantities, such as the differences of energy between the physical system of interest and the reference system can be evaluated accurately, even for the contribution to the energy differences in Ω^e. To see why this is possible, we first note that in the contour integral formulation, physical quantities, such as the the total number of electrons and total energy can be computed with the trace of differences of Green's functions, multiplied by the overlap matrix, i.e., $\mathrm{Tr}[SG - S^0 G^0]$. Note that both G and G^0 are z-dependent, and we have the identity

$$\mathrm{Tr}[GS] = \frac{d}{dz} \mathrm{Tr}\left[\log(zS - H)\right] = \frac{d}{dz} \log\det(zS - H),$$

and similarly

$$\mathrm{Tr}[G^0 S^0] = \frac{d}{dz} \log\det(zS^0 - H^0).$$

Here we used the identity $\mathrm{Tr}[\log(\cdot)] = \log[\det(\cdot)]$. Then we have

$$\begin{aligned}\mathrm{Tr}[GS] - \mathrm{Tr}[G^0 S^0] =& \frac{d}{dz} \log\det(G^0 G^{-1}) \\ =& \frac{d}{dz} \log\det(I - G^0 \Delta A) = \frac{d}{dz} \log\det(I_1 - G^0_{11}(\Delta A)_{11}),\end{aligned}$$

where we have used Dyson's equation for $G^0 G^{-1}$. In order to compute differences of energy, free energy or number of electrons, only the determinant of matrices restricted to $\Omega^i \cup \partial\Omega^e$ is needed. In practice the $\frac{d}{dz}$ operator can be approximated using a finite difference scheme in the complex plane.

The disadvantage of the Dyson equation approach is that the matrix G^0 in Eq. (18) is a dense matrix. Hence dense linear algebra must be used for matrix-matrix multiplication and matrix inversion operations. The computational cost can still be large when a large degree of freedom in Ω^i is needed.

3.3. **PEXSI-Σ method.** Let us now introduce the PEXSI-Σ method, which is our new strategy of treating the boundary conditions for the Green's function. Compared to previous schemes, our approach has the following advantages: 1) It is an accurate reformulation of the embedding scheme under the same assumption of the non-zero pattern of ΔA as that for the Dyson equation approach. Hence the reference Green's function G^0 can correspond to a physical reference system, such as the crystalline configuration. 2) The reduced system introduces a dense modification matrix *only* near the boundary, and hence the reduced system remains to be a sparse system for systems of large sizes. Such sparsity structure ensures that the computational complexity is still at most $\mathcal{O}(N^2)$ where N is the number of degrees of freedom corresponding to $\Omega^i \cup \partial\Omega^e$.

We first note that A^0 and A only differ in the A_{11} block as in Eq. (16), and the same Schur complement Σ as in Eq. (15) also appears in the equation for G^0

$$G^0_{11}(A^0_{11} + \Sigma) = I_1,$$

or equivalently

$$G^0_{11}\Sigma = I_1 - G^0_{11}A^0_{11}. \tag{19}$$

Here we demonstrate that Eq. (19) can be used to give a compact representation for Σ. Let us split the collective index 1 into (α, β), where the indices α, β denote the collective degrees of freedom for Ω^i and $\partial\Omega^e$, respectively. Then Eq. (19) can be written as

$$\begin{pmatrix} G^0_{\alpha\alpha} & G^0_{\alpha\beta} \\ G^0_{\beta\alpha} & G^0_{\beta\beta} \end{pmatrix} \begin{pmatrix} 0 & 0 \\ 0 & \Sigma_{\beta\beta} \end{pmatrix} = I_1 - G^0_{11}A^0_{11}. \tag{20}$$

Here we have used the fact that Σ only has non-zero component on the boundary degrees of freedom. Take the (β, β) component of the equation (20), and we have

$$G^0_{\beta\beta}\Sigma_{\beta\beta} = I_\beta - G^0_{\beta\alpha}A^0_{\alpha\beta} - G^0_{\beta\beta}A^0_{\beta\beta},$$

or in a more compact form

$$\Sigma_{\beta\beta} = (G^0_{\beta\beta})^{-1}(I - G^0_{\beta\alpha}A^0_{\alpha\beta}) - A^0_{\beta\beta}. \tag{21}$$

Compared to the Dyson equation approach, the advantage of using Eq. (21) is that the computation of the self energy Σ only depends on boundary degrees of freedom. For large

systems, the update to A_{11} due to Σ is localized on the boundary degrees of freedom $\partial\Omega^e$. As discussed in section 2, the asymptotic complexity of the selected inversion method comes from the size of the largest dense matrix block in the Cholesky factor L. For a finite size system, the size of this matrix block is approximately the same as the number of degrees of freedom corresponding to the surface of the system. Using the terminology in sparse linear algebra, we can reorder the matrix $A = zS - H$ so that the interior degrees of freedom Ω^i appear before the boundary degrees of freedom $\partial\Omega_e$. The Σ matrix only modifies the matrix block corresponding to degrees freedom in $\partial\Omega_e$. This matrix block becomes dense anyway, since it is the last block in the Gaussian elimination procedure (or LDL^T factorization). Therefore if number of degrees of freedom in Ω^i is sufficiently large, the modification due to Σ only increases the prefactor of the asymptotic complexity of selected inversion, which is at most $\mathcal{O}(N^2)$ and N is the number of degrees of freedom corresponding to $\Omega^i \cup \partial\Omega^e$.

With G_{11} computed, physical observables that relies on the local density matrix, such as the atomic force, can be readily computed. In PEXSI, the Hellmann-Feynman force associated with the I-th atom is given by [48]

$$F_I = -\mathrm{Tr}\left[\Gamma \frac{\partial H}{\partial R_I}\right] + \mathrm{Tr}\left[\Gamma^E \frac{\partial S}{\partial R_I}\right]. \tag{22}$$

Analogous to the density matrix (7), Γ^E is the energy density matrix defined by

$$\Gamma^E = C\Xi f_\beta(\Xi - \mu)C^T. \tag{23}$$

It has been shown that the energy density matrix can be computed using the same set of Green's function G_l as required for the density matrix, but with different weights $\{\omega_l^E\}$ [34]

$$\Gamma^E \approx \mathrm{Im}\ \left(C \sum_{l=1}^{P} \frac{\omega_l^E}{\Xi - (z_l + \mu)I} C^T\right) = \mathrm{Im}\ \left(\sum_{l=1}^{P} \frac{\omega_l^E}{(z_l + \mu)S - H}\right). \tag{24}$$

Note that the sparsity pattern of $\dfrac{\partial H}{\partial R_I}, \dfrac{\partial S}{\partial R_I}$ is the same as that of H, S respectively. Therefore if I corresponds to an atom in Ω^i, the trace in Eq. (22) can be computed using Γ, Γ^E restricted to $\Omega^i \cup \partial\Omega^e$, which is readily computed in the PEXSI-Σ formulation.

In order to evaluate the energy or the number of electrons in the global domain, one needs to either use exterior degrees of freedom explicitly, or to use the approach described in Eq. (19) for Dyson's equation, which we will not go into details here. On the other hand, PEXSI-Σ can be immediately used to evaluate the number of electrons restricted to Ω^i, denoted by N_e^i, which is a useful quantity to measure in charge transfer processes. Note that the global number of electrons can be computed as $N_e = \mathrm{Tr}[S\Gamma]$, the interior number of electrons can be computed as

$$N_e^i = \mathrm{Tr}[S_{\alpha\alpha}\Gamma_{\alpha\alpha}] + \mathrm{Tr}[S_{\alpha\beta}\Gamma_{\beta\alpha}]. \tag{25}$$

Similarly one can measure the interior band energy

$$E_{\mathrm{band}}^i = \mathrm{Tr}[S_{\alpha\alpha}\Gamma_{\alpha\alpha}^E] + \mathrm{Tr}[S_{\alpha\beta}\Gamma_{\beta\alpha}^E], \tag{26}$$

which is the contribution of the total band energy $E_{\mathrm{band}} = \mathrm{Tr}[S\Gamma^E]$ from the interior degrees of freedom.

4. Geometric relaxation by atomistic Green's function

Another appealing aspect of the present approach is that the relaxation of the nuclei can be formulated within the same framework. In mechanics, in order to predict structural properties of lattice defects, the surrounding atoms have to be relaxed so that the system reaches a mechanical equilibrium. In principle, the forces on every atom can be computed based on the Hellmann-Feynman theorem. With the same observation that away from the defects, the lattice deformation is small, we linearize the atomic interaction in the exterior region. This standard approximation is known as the harmonic approximation [2], under which the force balance can be expressed as a linear system of finite difference equations,

$$f_I \overset{\text{def}}{=} \sum_J D_{I,J}(u_I - u_J) = 0, \qquad \forall\, I \in \Omega^e, \tag{27}$$

subject to boundary conditions from the interior region. Here $D_{I,J}$ is the force constant matrix corresponding to the periodic lattice structure, defined as the second derivative of the energy. In the context of QM/MM coupling, such approximation has also been used in [7]. The force constant matrix $D_{I,J}$ can be computed by means of a finite difference approach (also called the "frozen phonon approach") in electron structure software packages. Since they are defined for a crystalline structure, a supercell can be used for this purpose. Similar to the sparsity of the matrices H and S, we will make a truncation for $D_{I,J}$ based on the magnitude of the matrix, and denote the spatial cutoff by r_{cut}. Notice that here we have assumed a same partition of the domain into Ω^i and Ω^e as in the electronic part. However, depending on the truncation radius, the sparsity of D might be different compared to the Hamiltonian matrix H. Therefore we denote the boundary by $\partial\Omega^e_{\text{atom}}$, as opposed to the definition of the boundary for the electron part, which was denoted by $\partial\Omega^e$.

Let us now show that similar to the electron part, the atom relaxation can be determined using a more efficient procedure so that atomic degrees of freedom can be restricted to the boundary. To see how this reduced model is derived, we use the matrix representation and denote u_α, u_β, and u_2 the displacement in the inner region Ω^i, outer boundary $\partial\Omega^e_{\text{atom}}$ and exterior $\Omega^e \backslash \partial\Omega^e_{\text{atom}}$, respectively. Then the force balance equations (27) can be rewritten as

$$D_{\beta\beta}u_\beta + D_{\beta 2}u_2 = -D_{\beta\alpha}u_\alpha, \quad D_{2\beta}u_\beta + D_{22}u_2 = 0. \tag{28}$$

The goal is to eliminate u_2. By the definition of the lattice Green's function $\mathcal{G}$ and the assumption that $D_{\alpha 2} = 0$, we have

$$\mathcal{G}_{\beta\alpha}D_{\alpha\beta} + \mathcal{G}_{\beta\beta}D_{\beta\beta} + \mathcal{G}_{\beta 2}D_{2\beta} = I, \quad \mathcal{G}_{\beta\beta}D_{\beta 2} + \mathcal{G}_{\beta 2}D_{22} = 0. \tag{29}$$

This simplifies Eq. (28) to

$$u_\beta = \mathcal{G}_{\beta\alpha}D_{\alpha\beta}u_\beta - \mathcal{G}_{\beta\beta}D_{\beta\alpha}u_\alpha. \tag{30}$$

This forms a closed system for the displacement of the atoms at the boundary. The coefficients in this linear system involve the force constant matrices and the Green's function for the reference state. Such equations have been derived and implemented in [31, 32] as a coarse-grained molecular mechanics model. There are various techniques for computing the Green's functions efficiently [43, 50].

The geometric optimization can be obtained as follows: For the atoms in Ω^i, the forces are determined from the KSDFT model, and the atomic positions are relaxed using a nonlinear solver, e.g., the conjugate-gradient method. These updated positions will be used as input in the Eq. (30), which becomes a closed linear system for the displacement of the atoms in $\partial\Omega^e_{\text{atom}}$. Once the displacement along $\partial\Omega^e_{\text{atom}}$ is determined from (30), this equation

can be used to evaluate the displacement of the atoms that are further out (e.g., those in $\Omega^e \backslash \partial\Omega^e_{\text{atom}}$).

Note that in this procedure the atomic degrees of freedom in Ω^e are completely determined by those in Ω^i. Due to our choice of the reference system to be the periodic lattice for A^0, in the current method, there is no feedback of the deformation of the exterior domain to the Ω^i. It would be an interesting future direction to consider how to incorporate the change into the reference Hamiltonian.

5. Numerical results

In this section we demonstrate the accuracy of the PEXSI-Σ method using three examples: a water dimer, a graphene system with a divacancy, and a graphene system with a dislocation dipole with opposite Burgers vectors under relaxed atomic configuration. Our method is implemented in the DFTB+ code [1]. DFTB+ uses the density functional tight binding (DFTB) method, which can be viewed as a numerical discretization of the Kohn-Sham density equations with minimal degrees of freedom, and thus allows the study of systems of relatively larger sizes without parallel implementation. DFTB+ defines a semi-empirical charge density, which can be computed both self-consistently and non-self-consistently. In the PEXSI-Σ method, self-consistent charge density calculation requires the charge density in Ω^e to be properly taken into account, which is not yet in the scope of this work. Hence all calculations below are performed in the non-self-consistent mode of DFTB+. In all calculations, the electronic temperature is set to the room temperature 300K. All quantities are reported in atomic units (au) unless otherwise specified. All the computation is performed on a single Intel i7 CPU processor with 64 gigabytes (GB) of memory.

We report the results for the following methods. For the full system, we compare the results from the exact diagonalization (DIAG) method and the pole expansion with selected inversion (PEXSI) method. We demonstrate that the results from DIAG and PEXSI fully agree with each other. When the exterior degrees of freedom are not taken into account directly, we use the PEXSI-Σ method. In order to demonstrate the effectiveness of the environment-dependent self energy matrix Σ, we also compare with the results by setting Σ to a zero matrix. This is referred to as the PEXSI-($\Sigma = 0$) method in this section. In the non-self-consistent calculations, the PEXSI-($\Sigma = 0$) method is equivalent to considering an isolated system with the degrees of freedom in Ω^e directly eliminated from the calculation. This is similar to setting a "vacuum boundary condition" for the interior degrees of freedom together with the buffer region. In all the examples, we find that the inclusion of a properly approximated Σ matrix significantly improves the accuracy.

5.1. **Water dimer.** Our first example is a water dimer system (Fig. 3). The system is partitioned into two parts, with one water molecule described as Ω^i and the other molecule as Ω^e. Here 80 poles are used in the PEXSI and PEXSI-Σ method to guarantee accuracy. At the equilibrium configuration, the total energy obtained from the DIAG method is -8.1705870965 au, and the total energy obtained from the PEXSI method is -8.1705870964 au, with discrepancy less than 10^{-10} au. Therefore the results from DIAG and PEXSI fully agree with each other.

In order to demonstrate that the PEXSI-Σ method gives accurate results in different atomic configurations, we stretch the water molecule in Ω^i along the oxygen-oxygen direction, and denote by Δd_{OO} the displacement away from equilibrium position. In the PEXSI-Σ method, the Hamiltonian matrix elements between Ω^i and Ω^e vary with respect to the change of the atomic configuration. Hence in the absence of the energy contribution

from Ω^e, the total energies obtained from PEXSI and PEXSI-Σ in general do not agree with each other. However, as discussed in section 3.3, the interior band energy E^i_{band}, together with the atomic force corresponding to atoms in Ω^i should agree well between PEXSI and PEXSI-Σ .

Fig. 3 (a), (b) report the interior band energy, as well as the force on the oxygen atom in Ω^i projected along the O-O direction, respectively. We find that energies and forces vary smoothly with respect to the change of the O-O distance, and the results from PEXSI and PEXSI-Σ fully agree with each other. We remark that due to the small system size, the exterior degrees of freedom Ω^e coincide with the boundary degrees of freedom $\partial\Omega^e$. Hence all Σ matrices are zero. In this special case, the PEXSI-Σ method and the PEXSI-($\Sigma = 0$) method are the same.

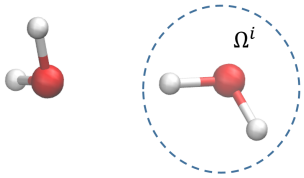

FIGURE 3. Atomic configuration for water dimer. Large red ball: oxygen (O). Small white ball: hydrogen (H). The molecule in Ω^i is stretched along the O-O direction.

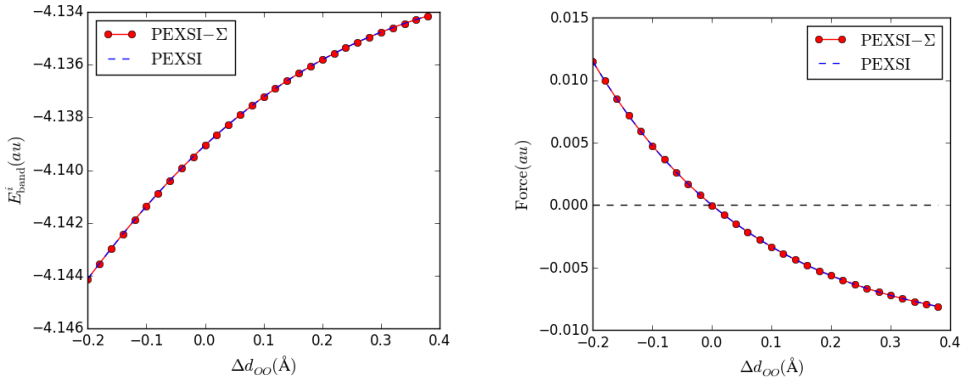

FIGURE 4. (a) The interior band energy, and (b) the force on the oxygen atom in Ω^i projected along the O-O direction, as the molecule in Ω^i is stretched along the O-O direction.

5.2. **Divacancy in graphene.** Our second numerical example is a graphene system with a single divacancy defect. Starting from a periodic configuration with 420 atoms, two atoms are removed to create a divacancy (Fig. 5). No further structural relaxation is performed at this stage. In the periodic configuration without the defect, the total energy computed from the DIAG method is -721.049897496 au, and the total energy computed from the PEXSI

method with 80 poles and at the same chemical potential is -721.049897489 au. Hence the results from DIAG and PEXSI fully agree with each other, and all numerical results below will be benchmarked with that from the PEXSI method.

For the divacancy system, the atoms are partitioned according to Fig. 5. Since $\Omega^e \backslash \partial\Omega^e$ is non-empty, the Σ matrices are non-zero. In the PEXSI-Σ method, the Σ matrices are obtained from the PEXSI calculation in the periodic configuration. We compare the interior band energy between the divacancy (D) and periodic configuration (P) in Table 1, obtained from PEXSI, PEXSI-Σ , and PEXSI-($\Sigma = 0$) methods, respectively. In order to assess the relative accuracy of the methods, we also compare the interior band energy for another system by shifting one atom in Fig. 5 by a small distance of 0.1 Å along the x-direction. The resulting configuration is denoted by SD (shifted divacancy, Fig. 6).

Table 1 indicates that in the periodic configuration, the result from PEXSI-Σ fully agrees with that from PEXSI. Even though the Σ matrix is obtained from the periodic configuration, the inclusion of Σ matrices in the PEXSI-Σ formulation significantly improves the accuracy in other atomic configurations as well. The error of the energy difference between the divacancy and periodic configuration using the PEXSI-($\Sigma = 0$) method is 0.0145 au. This error is reduced by 67 times to 0.0002 au in the PEXSI-Σ method. Similarly the error of the energy difference between the divacancy and the shifted divacancy configuration using the PEXSI-($\Sigma = 0$) method is 0.0027 au, and the error is reduced by about 75 times to 0.000036 au in the PEXSI-Σ method.

We report the maximum of the error of the atomic forces calculated from all interior atoms in Table 2. In all configurations, the maximum force error obtained from the PEXSI-Σ method is less than 3×10^{-5} au, which is very accurate for geometry optimization and molecular dynamics studies. Compared to the PEXSI-($\Sigma = 0$) method, the improvement due to the inclusion of the Σ matrix is again nearly 2 orders of magnitude.

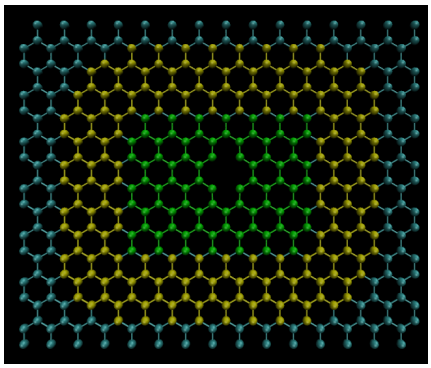

FIGURE 5. Atomic configuration of the divacancy example in graphene with 418 atoms, partitioned into interior atoms Ω^i (green), boundary atoms $\partial\Omega^e$ (yellow), and the rest of the exterior atoms $\Omega^e \backslash \partial\Omega^e$ (cyan).

5.3. **Dislocation dipole in graphene.** In this test problem, we consider a dislocation dipole in the graphene system. Such a dislocation can be identified as a pentagon-heptagon (5-7) pairs among the hexagonal rings [4]. As comparison, we form a supercell with 720 atoms in total. The entire system is 4.55nm×4.38nm. Fig. 7 (a) shows the atomic configuration as well as the partition of the system. Compared to the example in section 5.2, the

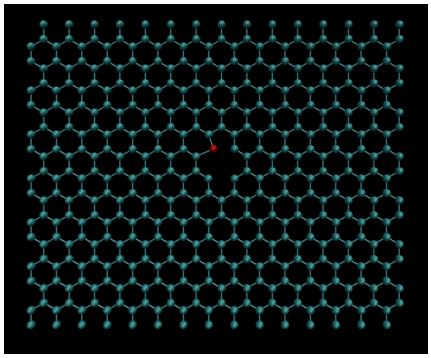

FIGURE 6. Atomic configuration of the divacancy system with one atom (red) shifted by 0.1 Å along the x-direction. The same partitioning strategy as in Fig. 5 is used.

System	PEXSI	PEXSI-Σ	PEXSI-($\Sigma = 0$)
Periodic (P)	-145.70244	-145.70244	-145.76624
Divacancy (D)	-142.56345	-142.56367	-142.61273
Shifted Divacancy (SD)	-142.45347	-142.45368	-142.50003
Energy difference (D-P)	3.13899	3.13877	3.15351
Energy difference (SD-D)	0.10999	0.11003	0.11270

TABLE 1. The interior band energy for the graphene systems. Unit: au

System	PEXSI-Σ	PEXSI-($\Sigma = 0$)
Periodic (P)	0.00000	0.00407
Divacancy (D)	0.00003	0.00399
Shifted Divacancy (SD)	0.00003	0.00384

TABLE 2. Maximum error of the force for interior degrees of freedom for the graphene systems. Unit: au

interior domain is reduced to be just around the dislocation dipole. Structural relaxation is also performed for the entire system so that all atoms, including the atoms in the exterior domain, deviate from the equilibrium position, as shown in Fig. 7 (b). The Σ matrix is still constructed from the graphene system with periodic structure. Fig. 8 shows that even with a small interior domain and deformed atomic configuration in the exterior domain, the accuracy of PEXSI-Σ reduces the error of the force uniformly for all atoms in the interior domain to be around 10^{-3} au.

6. Conclusion and future work

In this work we proposed a new Green's function embedding method called PEXSI-Σ for efficient treatment of boundary conditions in complex materials. The Σ matrices can be constructed using Green's functions corresponding to any physical reference system that shares a similar potential corresponding to exterior degrees of freedom. The Σ matrices can

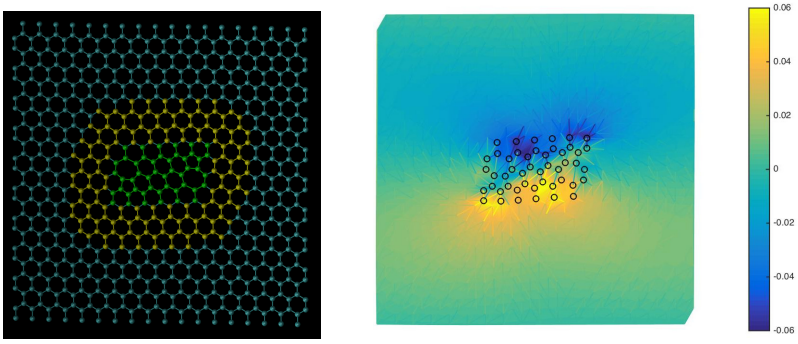

FIGURE 7. (Left) Atomic configuration of the dislocation dipole example with 720 atoms, partitioned into interior atoms Ω^i (green), boundary atoms $\partial\Omega^e$ (yellow), and the rest of the exterior atoms $\Omega^e \backslash \partial\Omega^e$ (cyan). (Right) Displacement field (first component) after the geometric relaxation; the position of interior atoms is plotted on top.

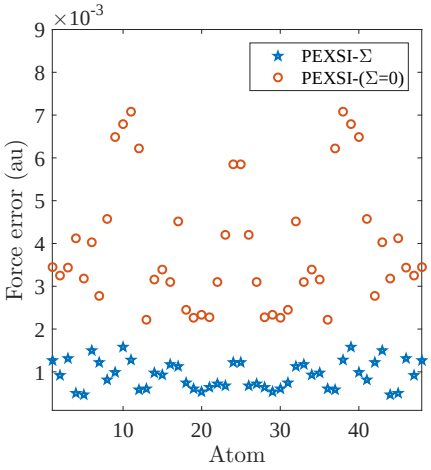

FIGURE 8. Error of the atomic force for atoms in the interior domain of the dislocation dipole system.

be viewed as a surface potential and do not introduce additional interaction among the interior degrees of freedom. Hence for systems with large number of interior degrees of freedom, the calculation can be performed efficiently using the pole expansion and selected inversion method (PEXSI). Numerical results using non-self-consistent DFTB+ calculations for water dimer, graphene with divacancy and graphene with dislocation dipole demonstrated the accuracy of the method.

We note that our current implementation of the PEXSI-Σ method, which is only serial, is just a proof of principle. As indicated by the performance of the PEXSI method [24, 35], when the number of interior degrees of freedom is large, the PEXSI-Σ method should readily allow a massively parallel implementation in the future with at most $\mathcal{O}(N^2)$ complexity. In order to apply the PEXSI-Σ method for the accurate computation of physical quantities, we

need to include the self-consistent field effect, which requires the solution of a Coulomb-like equation on the global domain. In particular, the electrostatic energy depends sensitively on the total number of electrons in the system. It is most natural to use a fixed chemical potential. This corresponds to the grand canonical ensemble in the PEXSI-Σ method, and may be a more natural choice for describing processes with charge transfer. However, the grand canonical ensemble treatment might need to be relaxed when the reference system is of finite size. The Σ matrices are constructed from G^0, which is only exact in the absence of deformation of exterior degrees of freedom. When the potential in the exterior domain changes due to atomic relaxation or long range Coulomb interaction, the correction to the Σ matrix could be possibly computed by means of perturbation theory. We also remark that Green's function embedding methods may also become more versatile if the Σ matrices exhibit certain locality properties to accommodate structural changes of atoms in the exterior domain such as in the presence of a single dislocation, and also can be used to study interaction of defects by using multiple disconnected QM regions. Green's function embedding methods may also be an attractive alternative for coupling with electronic structure theories beyond the level of KSDFT (see e.g., the recent works [8, 58]). We plan to explore these directions in the future.

References

[1] B. Aradi, B. Hourahine, and T. Frauenheim, *DFTB+, a sparse matrix-based implementation of the DFTB method*, J. Phys. Chem. A **111** (2007), 5678–5684.

[2] N. W. Ashcroft and N. D. Mermin, *Solid state physics*, Brooks Cole, 1976.

[3] J. Bernholc, N. O. Lipari, and S. T. Pantelides, *Self-consistent method for point defects in semiconductors: Application to the vacancy in silicon*, Phys. Rev. Lett. **41** (1978), 895.

[4] L. L. Bonilla and A. Carpio, *Driving dislocations in graphene*, Science **337** (2012), 161–162.

[5] M. Brandbyge, J.-L. Mozos, P. Ordejón, J. Taylor, and K. Stokbro, *Density-functional method for nonequilibrium electron transport*, Phys. Rev. B **65** (2002), 165401.

[6] E. Brunk and U. Rothlisberger, *Mixed quantum mechanics/molecular mechanical molecular dynamics simulations of biological systems in ground and electronically excited states*, Chem. Rev. **115** (2015), 6217–6263.

[7] H. Chen and C. Ortner, *QM/MM methods for crystalline defects. Part 2: Consistent energy and force-mixing*, arXiv:1509.06627 (2015).

[8] W. Chibani, X. Ren, M. Scheffler, and P. Rinke, *Self-consistent Green's function embedding for advanced electronic structure methods based on a dynamical mean-field concept*, Phys. Rev. B **93** (2016), 165106.

[9] P. Cortona, *Self-consistently determined properties of solids without band-structure calculations*, Phys. Rev. B **44** (1991), 8454.

[10] B. Engquist and A. Majda, *Absorbing boundary conditions for numerical simulation of waves*, Proc. Natl. Acad. Sci. **74** (1977), 1765–1766.

[11] J. Gao and D. G. Truhlar, *Quantum mechanical methods for enzyme kinetics*, Annu. Rev. Phys. Chem. **53** (2002), 467–505.

[12] C.J. García-Cervera, J. Lu, and W. E, *Asymptotics-based sub-linear scaling algorithms and application to the study of the electronic structure of materials*, Commun. Math. Sci. **5** (2007), 999–1024.

[13] D. Givoli, I. Patlashenko, and J. B. Keller, *Discrete Dirichlet-to-Neumann maps for unbounded domains*, Comput. Methods Appl. Mech. Engrg. **164** (1998), 173–185.

[14] S. Goedecker, *Integral representation of the Fermi distribution and its applications in electronic-structure calculations*, Phys. Rev. B **48** (1993), 17573.

[15] ———, *Linear scaling electronic structure methods*, Rev. Mod. Phys. **71** (1999), 1085–1123.

[16] J. D. Goodpaster, N. Ananth, F. R. Manby, and T. F. Miller III, *Exact nonadditive kinetic potentials for embedded density functional theory*, J. Chem. Phys. **133** (2010), 084103.

[17] P. Hohenberg and W. Kohn, *Inhomogeneous electron gas*, Phys. Rev. **136** (1964), B864–B871.

[18] W. Hu, L. Lin, and C. Yang, *DGDFT: A massively parallel method for large scale density functional theory calculations*, J. Chem. Phys. **143** (2015), 124110.

[19] W. Hu, L. Lin, C. Yang, J. Dai, and J. Yang, *Edge-modified phosphorene nanoflake heterojunctions as highly efficient solar cells*, Nano Lett. **16** (2016), 1675.
[20] W. Hu, L. Lin, C. Yang, and J. Yang, *Electronic structure of large-scale graphene nanoflakes*, J. Chem. Phys. **141** (2014), 214704.
[21] C. Huang, M. Pavone, and E. A. Carter, *Quantum mechanical embedding theory based on a unique embedding potential*, J. Chem. Phys. **134** (2011), 154110.
[22] J. E. Inglesfield, *A method of embedding*, J. Phys. C **14** (1981), 3795.
[23] M. Jacquelin, L. Lin, N. Wichmann, and C. Yang, *Enhancing the scalability and load balancing of the parallel selected inversion algorithm via tree-based asynchronous communication*, IPDPS, accepted (2016).
[24] M. Jacquelin, L. Lin, and C. Yang, *PSelInv–a distributed memory parallel algorithm for selected inversion: the symmetric case*, ACM Trans. Math. Software **accepted** (2015).
[25] J. B. Keller and D. Givoli, *Exact non-reflecting boundary conditions*, J. Comput. Phys. **82** (1989), 172–192.
[26] P. J. Kelly and R. Car, *Green's-matrix calculation of total energies of point defects in silicon*, Phys. Rev. B **45** (1992), 6543.
[27] G. Knizia and G. K.-L. Chan, *Density matrix embedding: A strong-coupling quantum embedding theory*, J. Chem. Theory Comput. **9** (2013), 1428–1432.
[28] W. Kohn, *Density functional and density matrix method scaling linearly with the number of atoms*, Phys. Rev. Lett. **76** (1996), 3168–3171.
[29] W. Kohn and L. Sham, *Self-consistent equations including exchange and correlation effects*, Phys. Rev. **140** (1965), A1133–A1138.
[30] G. Kresse and J. Furthmüller, *Efficient iterative schemes for ab initio total-energy calculations using a plane-wave basis set*, Phys. Rev. B **54** (1996), 11169–11186.
[31] X. Li, *Efficient boundary condition for molecular statics models of solids*, Phys. Rev. B **80** (2009), 104112.
[32] ———, *An atomistic-based boundary element method for the reduction of molecular statics models*, Comput. Methods Appl. Mech. Engrg. **225** (2012), 1–13.
[33] H. Lin and D. G. Truhlar, *QM/MM: what have we learned, where are we, and where do we go from here?*, Theor. Chem. Acc. **177** (2007), 185–199.
[34] L. Lin, M. Chen, C. Yang, and L. He, *Accelerating atomic orbital-based electronic structure calculation via pole expansion and selected inversion*, J. Phys. Condens. Matter **25** (2013), 295501.
[35] L. Lin, A. García, G. Huhs, and C. Yang, *SIESTA-PEXSI: Massively parallel method for efficient and accurate ab initio materials simulation without matrix diagonalization*, J. Phys.: Condens. Matter **26** (2014), 305503.
[36] L. Lin, J. Lu, L. Ying, R. Car, and W. E, *Fast algorithm for extracting the diagonal of the inverse matrix with application to the electronic structure analysis of metallic systems*, Comm. Math. Sci. **7** (2009), 755.
[37] L. Lin, J. Lu, L. Ying, and W. E, *Pole-based approximation of the Fermi-Dirac function*, Chin. Ann. Math. **30B** (2009), 729.
[38] ———, *Adaptive local basis set for Kohn-Sham density functional theory in a discontinuous Galerkin framework I: Total energy calculation*, J. Comput. Phys. **231** (2012), 2140–2154.
[39] L. Lin, C. Yang, J. Meza, J. Lu, L. Ying, and W. E, *SelInv – An algorithm for selected inversion of a sparse symmetric matrix*, ACM. Trans. Math. Software **37** (2011), 40.
[40] M. P Lopez-Sancho, J. M. Lopez-Sancho, and J. Rubio, *Quick iterative scheme for the calculation of transfer matrices: application to Mo (100)*, J. Phys. F **14** (1984), 1205.
[41] G.D. Mahan, *Many-particle Physics*, Plenum Pub Corp, 2000.
[42] G. Makov and M. C. Payne, *Periodic boundary conditions in ab initio calculations*, Phys. Rev. B **51** (1995), 4014.
[43] P. G. Martinsson and G. J. Rodin, *Asymptotic expansions of lattice Green's functions*, Proc. R. Soc. Lond. A **458** (2002), 2609–2622.
[44] S. Mohr, L. E. Ratcliff, P. Boulanger, L. Genovese, D. Caliste, T. Deutsch, and S. Goedecker, *Daubechies wavelets for linear scaling density functional theory*, J. Chem. Phys. **140** (2014), 204110.
[45] D. M. C. Nicholson, G. M. Stocks, Y. Wang, W. A. Shelton, Z. Szotek, and W. M. Temmerman, *Stationary nature of the density-functional free energy: Application to accelerated multiple-scattering calculations*, Phys. Rev. B **50** (1994), 14686.

[46] M. C. Payne, M. P. Teter, D. C. Allen, T. A. Arias, and J. D. Joannopoulos, *Iterative minimization techniques for* ab initio *total energy calculation: molecular dynamics and conjugate gradients*, Rev. Mod. Phys. **64** (1992), 1045–1097.
[47] H. M. Senn and W. Thiel, *QM/MM methods for biomolecular systems*, Angew. Chem. Int. Ed. Engl. **48** (2009), 1198–1229.
[48] J. M. Soler, E. Artacho, J. D. Gale, A. García, J. Junquera, P. Ordejón, and D. Sánchez-Portal, *The SIESTA method for ab initio order-N materials simulation*, J. Phys.: Condens. Matter **14** (2002), 2745–2779.
[49] A. Thiess, R. Zeller, M. Bolten, P. H. Dederichs, and S. Blügel, *Massively parallel density functional calculations for thousands of atoms: KKRnano*, Phys. Rev. B **85** (2012), 235103.
[50] D. R. Trinkle, *Lattice Green function for extended defect calculations: Computation and error estimation with long-range forces*, Phys. Rev. B **78** (2008), 014110.
[51] J. VandeVondele, M. Krack, F. Mohamed, M. Parrinello, T. Chassaing, and J. Hutter, *QUICKSTEP: Fast and accurate density functional calculations using a mixed gaussian and plane waves approach*, Comput. Phys. Commun. **167** (2005), 103.
[52] Y. Wang, G. M. Stocks, W. A. Shelton, D. M. C. Nicholson, Z. Szotek, and W. M. Temmerman, *Order-N multiple scattering approach to electronic structure calculations*, Phys. Rev. Lett. **75** (1995), 2867.
[53] A. Warshel and M. Levitt, *Theoretical studies of enzymic reactions: dielectric, electrostatic and steric stabilization of the carbonium ion in the reaction of lysozyme*, J. Mol. Biol. **103** (1976), 227–249.
[54] A. R. Williams, P. J. Feibelman, and N. D. Lang, *Green's-function methods for electronic-structure calculations*, Phys. Rev. B **26** (1982), 5433.
[55] R. Zeller and P. H. Dederichs, *Electronic Structure of Impurities in Cu, Calculated Self-Consistently by Korringa-Kohn-Rostoker Green's-Function Method*, Phys. Rev. Lett. **42** (1979), 1713.
[56] R. Zeller, P. H. Dederichs, B. Ujfalussy, L. Szunyogh, and P. Weinberger, *Theory and convergence properties of the screened Korringa-Kohn-Rostoker method*, Phys. Rev. B **52** (1995), 8807.
[57] R. Zeller, J. Deutz, and P.H. Dederichs, *Application of complex energy integration to selfconsistent electronic structure calculations*, Solid State Commun. **44** (1982), 993–997.
[58] D. Zgid and G. K.-L. Chan, *Dynamical mean-field theory from a quantum chemical perspective*, J. Chem. Phys. **134** (2011), 094115.

Department of Mathematics, The Pennsylvania State University, University Park, PA 16802
E-mail address: xxl12@psu.edu

Department of Mathematics, University of California, Berkeley and Computational Research Division, Lawrence Berkeley National Laboratory, Berkeley CA 94720 USA
E-mail address: linlin@math.berkeley.edu

Department of Mathematics, Department of Physics, and Department of Chemistry, Duke University, Durham, NC 27708 USA
E-mail address: jianfeng@math.duke.edu